AIAA JOURNAL
Vol. 41, No. 9, September 2003

Micromechanics-Based Modeling of Woven Polymer Matrix Composites

Brett A. Bednarcyk*
Ohio Aerospace Institute, Brookpark, Ohio 44142
and
Steven M. Arnold†
NASA John H. Glenn Research Center at Lewis Field, Cleveland, Ohio 44135

A novel approach is combined with the generalized method of cells (GMC) to predict the elastic properties of plain-weave polymer matrix composites (PMCs). The traditional one-step three-dimensional homogenization procedure that has been used in conjunction with GMC for modeling woven composites in the past is inaccurate due to the lack of shear coupling inherent in the model. However, by performing a two-step homogenization procedure in which the woven composite repeating unit cell is homogenized independently in the through-the-thickness direction prior to homogenization in the plane of the weave, GMC can now accurately model woven PMCs. This two-step procedure is outlined and implemented, and predictions are compared with results from the traditional one-step approach as well as other model and experimental results from the literature. Full coupling of this two-step technique within the recently developed Micromechanics Analysis Code with GMC software package will result in a widely applicable, efficient, and accurate tool for the design and analysis of woven composite materials and structures.

I. Introduction

COMPOSITES with woven reinforcements are attractive due to their ease of manufacture compared to unidirectional composites and laminates. Reinforcement preforms can be woven (or braided) into complex shapes that will remain intact prior to infiltration with the matrix material. This can reduce costs associated with machining because near-net-shaped components can be fabricated. Woven reinforcements are particularly effective in polymer matrix composites (PMCs) applications where cost is often a driving design factor.

The beneficial qualities of woven composites come at a cost in terms of analysis; their thermomechanical behavior is significantly more difficult to model due to the complex and inherently three-dimensional geometry associated with the woven reinforcement. Typically, woven composites have been modeled either by considering a simplified geometric representation and using homogenization techniques (usually isostress and isostrain assumptions) or via analysis of the actual three-dimensional geometry using finite element analysis (FEA). For recent reviews of such efforts, the reader is referred to Refs. 1 and 2. In general, the drawbacks of these approaches involve the accuracy of the predictions, geometric generality, computational efficiency, the ability to admit local (constituent-scale) submodels (i.e., viscoplasticity, damage, microfailure), or suitability to function in the framework of broader component-level analysis techniques. A notable exception to the preceding characterization is the binary model developed by Cox et al.[3] The binary model employs a nonlinear finite element approach in which complex three-dimensional woven (or braided) geometries are resolved into a number of stiff towline elements and compliant solid elements. Hence, the arbitrary composite geometry can be accurately captured while circumventing the cumbersome and computationally intensive three-dimensional mesh normally associated with FEA (for modeling complex weaves).

Another approach that overcomes many drawbacks related to previous woven-composite modeling efforts is the method of cells, developed by Aboudi.[4] The generalization of this model, the generalized method of cells (GMC),[5] and the three-dimensional triply periodic version of GMC[6] increased the breadth of applicability of the original method of cells considerably. The macroscale (composite-level) accuracy of GMC for modeling the thermomechanical behavior of continuous and discontinuous composites has been well established. GMC also admits arbitrary doubly and triply periodic geometries, making the method completely general with respect to geometry (provided a geometric repeating unit cell can be identified). In its original form, GMC was quite computationally efficient compared to FEA (see, e.g., Ref. 7); however, the efficiency of the method has been significantly increased via a reformulation by Pindera and Bednarcyk.[2,8] Similarly, because GMC provides efficient access to the local (constituent) stress and strain fields in simulated composite materials, it is ideal for inclusion of local submodels and, because it represents a material rather than a structure (such as a plate) it is well suited for implementation in higher scale analysis techniques such as FEA.[9,10]

Due to its useful aforementioned characteristics, GMC was selected as the foundation for NASA Glenn Research Center's Micromechanics Analysis Code with Generalized Method of Cells (MAC/GMC) software package.[9] This product is available to (and in use by) U.S. industry and universities for composite design and analysis.‡ MAC/GMC takes advantage of GMC's beneficial properties and provides many additional features such as 1) the ability to simulate arbitrary thermomechanical loading histories, 2) a library of geometric repeating unit cells, 3) user-definable subroutines, 4) damage and local failure modeling, 5) a library of elastic and viscoplastic material constitutive models, and 6) a seamless interface with the ABAQUS FEA package. Thus, MAC/GMC is an ideal candidate for modeling woven composite materials.

Received 5 February 2001; presented as Paper 2001-1567 at the AIAA/ASME/ASCE/AHS/ASC 42nd Structures, Structural Dynamics, and Materials Conference, Seattle, WA, 16–19 April 2001; revision received 15 June 2002; accepted for publication 10 December 2002.

*Senior Research Associate; also Senior Visiting Research Scientist, Department of Civil Engineering, University of Virginia, Charlottesville, VA 22904-4742. Member AIAA.

†Senior Research Engineer, Structures Division, Life Prediction Branch.

‡Data available online at http://www.grc.nasa.gov/WWW/LPB/mac [cited 18 July 2003].

Bednarcyk and Pindera[1,2] used GMC to model a woven carbon/copper (C/Cu) metal matrix composite (MMC). In these studies, the original method of cells was used to represent the unidirectional infiltrated fiber yarns embedded within the triply periodic version of GMC, thus enabling representation of the composite's three-dimensional repeating unit cell. Local submodels were incorporated to account for matrix plasticity and fiber–matrix debonding, allowing reasonably good agreement with mechanical experimental test data. However, due to GMC's inherent lack of coupling between the normal and shear stress and strain fields, the method has (until now) been unable to model PMCs accurately. In C/Cu MMCs, however, the dominant nature of the effects of matrix plasticity and fiber–matrix debonding muted the inaccuracies associated with GMC's lack of shear coupling, permitting reasonably accurate predictions for C/Cu systems. PMCs, on the other hand, are typically modeled elastically, and fiber–matrix debonding is often restricted to the near-failure regime of the PMC's response. Hence, GMC's predictions for the elastic properties of PMCs have been poor. With the inability to predict accurately the effective properties of PMCs (the most common form of woven composites), the usefulness of GMC in modeling woven composites could only be characterized as limited.

A concept that immediately exhibited potential for overcoming GMC's difficulties in accurately modeling woven PMCs was recently reported independently by Tabiei and Jiang[11] and Huang.[12] These authors presented approaches to model a plain-weave PMC in which, prior to homogenizing in the plane of the woven reinforcement, homogenization (via use of isostress and isostrain assumptions) was performed through the thickness of the weave. As will be shown, this two-step homogenization concept can be used in conjunction with GMC to enable accurate and consistent prediction of woven PMC elastic properties. Furthermore, in the context of a fully embedded approach to modeling general woven and braided composites like that presented by Bednarcyk and Pindera,[2,13] employing a through-the-thickness homogenization step (before homogenization in the plane of the weave, but after homogenization of the fiber and matrix to obtain the infiltrated yarn behavior) is clearly warranted.

II. GMC Mixed Concentration Equations

The reader is referred to Refs. 5 and 6 for full presentations of the doubly and triply periodic versions of GMC and to Refs. 8 and 2 for the corresponding reformulations. Here we will establish a theoretical background for the GMC equations based on the concept of mixed-concentration equations. Whereas the traditional stress and strain concentration equations relate local stresses to global stress and local strains to global strain, the desired mixed-concentration equations relate local stresses to global strain. Such mixed-concentration equations are essential in the reformulated version of GMC.

We begin with Hill's[14] stress and strain concentration equations including thermal and inelastic effects:

$$\boldsymbol{\sigma}^{(\alpha\beta\gamma)} = \boldsymbol{B}^{(\alpha\beta\gamma)}\bar{\boldsymbol{\sigma}} + \sum_{\lambda\xi\eta} \boldsymbol{B}_T^{(\alpha\beta\gamma,\lambda\xi\eta)}\boldsymbol{C}^{(\lambda\xi\eta)}\boldsymbol{\varepsilon}_T^{(\lambda\xi\eta)} + \sum_{\lambda\xi\eta} \boldsymbol{B}_I^{(\alpha\beta\gamma,\lambda\xi\eta)}\boldsymbol{C}^{(\lambda\xi\eta)}\boldsymbol{\varepsilon}_I^{(\lambda\xi\eta)} \tag{1}$$

$$\boldsymbol{\varepsilon}^{(\alpha\beta\gamma)} = \boldsymbol{A}^{(\alpha\beta\gamma)}\bar{\boldsymbol{\varepsilon}} + \sum_{\lambda\xi\eta} \boldsymbol{A}_T^{(\alpha\beta\gamma,\lambda\xi\eta)}\boldsymbol{\varepsilon}_T^{(\lambda\xi\eta)} + \sum_{\lambda\xi\eta} \boldsymbol{A}_I^{(\alpha\beta\gamma,\lambda\xi\eta)}\boldsymbol{\varepsilon}_I^{(\lambda\xi\eta)} \tag{2}$$

where $\boldsymbol{\sigma}^{(\alpha\beta\gamma)}$ and $\boldsymbol{\varepsilon}^{(\alpha\beta\gamma)}$ are the vectors of the six (average) stress and strain components, respectively, in a subvolume defined by the indices $(\alpha\beta\gamma)$; $\bar{\sigma}$ and $\bar{\varepsilon}$ are the average (global) stress and strain component vectors, respectively; $\boldsymbol{\varepsilon}_T^{(\lambda\xi\eta)}$ and $\boldsymbol{\varepsilon}_I^{(\lambda\xi\eta)}$ are the (average) thermal and inelastic strain vectors, respectively, in subvolume $(\lambda\xi\eta)$; and $\boldsymbol{C}^{(\lambda\xi\eta)}$ is the elastic stiffness matrix for subvolume $(\lambda\xi\eta)$. The familiar stress and strain concentration matrices for subvolume $(\alpha\beta\gamma)$ are $\boldsymbol{B}^{(\alpha\beta\gamma)}$ and $\boldsymbol{A}^{(\alpha\beta\gamma)}$, respectively. The inelastic and thermal strain distributions in each subvolume affect the stresses and strains in every other subvolume. Hence, the thermal and inelastic stress concentration matrices, $\boldsymbol{B}_T^{(\alpha\beta\gamma,\lambda\xi\eta)}$ and $\boldsymbol{B}_I^{(\alpha\beta\gamma,\lambda\xi\eta)}$, respectively, as well as the thermal and inelastic strain concentration matrices, $\boldsymbol{A}_T^{(\alpha\beta\gamma,\lambda\xi\eta)}$ and $\boldsymbol{A}_I^{(\alpha\beta\gamma,\lambda\xi\eta)}$, respectively, have the double-index superscripts. The summations appearing in Eqs. (1) and (2), $\Sigma_{\lambda\xi\eta}$, represent summation over all subvolumes denoted by $(\lambda\xi\eta)$.

The local constitutive equation for subvolume $(\alpha\beta\gamma)$ may be written

$$\boldsymbol{\sigma}^{(\alpha\beta\gamma)} = \boldsymbol{C}^{(\alpha\beta\gamma)}\left[\boldsymbol{\varepsilon}^{(\alpha\beta\gamma)} - \boldsymbol{\varepsilon}_T^{(\alpha\beta\gamma)} - \boldsymbol{\varepsilon}_I^{(\alpha\beta\gamma)}\right] \tag{3}$$

and the global (effective) constitutive equation is

$$\bar{\boldsymbol{\sigma}} = \boldsymbol{C}^*[\bar{\varepsilon} - \bar{\varepsilon}_T - \bar{\varepsilon}_I] \tag{4}$$

where, $\boldsymbol{C}^*$ is the effective elastic stiffness matrix and $\bar{\varepsilon}_T$ and $\bar{\varepsilon}_I$ are the global (average) thermal and inelastic strain vectors, respectively. The average stress vector is defined as

$$\bar{\boldsymbol{\sigma}} = \frac{1}{V}\sum_{\alpha\beta\gamma} V^{(\alpha\beta\gamma)}\boldsymbol{\sigma}^{(\alpha\beta\gamma)} \tag{5}$$

where V is the overall volume and $V^{(\alpha\beta\gamma)}$ is the volume of subvolume $(\alpha\beta\gamma)$.

Substituting Eq. (3) into Eq. (5) yields

$$\bar{\boldsymbol{\sigma}} = \frac{1}{V}\sum_{\alpha\beta\gamma} V^{(\alpha\beta\gamma)}\boldsymbol{C}^{(\alpha\beta\gamma)}\left[\boldsymbol{\varepsilon}^{(\alpha\beta\gamma)} - \boldsymbol{\varepsilon}_T^{(\alpha\beta\gamma)} - \boldsymbol{\varepsilon}_I^{(\alpha\beta\gamma)}\right] \tag{6}$$

and substituting Eq. (2) into Eq. (6) gives

$$\bar{\boldsymbol{\sigma}} = \frac{1}{V}\sum_{\alpha\beta\gamma} V^{(\alpha\beta\gamma)}\boldsymbol{C}^{(\alpha\beta\gamma)}\left[\boldsymbol{A}^{(\alpha\beta\gamma)}\bar{\boldsymbol{\varepsilon}} + \sum_{\lambda\xi\eta}\boldsymbol{A}_T^{(\alpha\beta\gamma,\lambda\xi\eta)}\boldsymbol{\varepsilon}_T^{(\lambda\xi\eta)} - \boldsymbol{\varepsilon}_T^{(\alpha\beta\gamma)} + \sum_{\lambda\xi\eta}\boldsymbol{A}_I^{(\alpha\beta\gamma,\lambda\xi\eta)}\boldsymbol{\varepsilon}_I^{(\lambda\xi\eta)} - \boldsymbol{\varepsilon}_I^{(\alpha\beta\gamma)}\right] \tag{7}$$

Comparing Eq. (7) with Eq. (4) allows the identification of the global or effective terms appearing in Eq. (4), namely

$$\boldsymbol{C}^* = \frac{1}{V}\sum_{\alpha\beta\gamma} V^{(\alpha\beta\gamma)}\boldsymbol{C}^{(\alpha\beta\gamma)}\boldsymbol{A}^{(\alpha\beta\gamma)} \tag{8}$$

$$\bar{\boldsymbol{\varepsilon}}_T = \frac{[\boldsymbol{C}^*]^{-1}}{V}\sum_{\alpha\beta\gamma} V^{(\alpha\beta\gamma)}\boldsymbol{C}^{(\alpha\beta\gamma)}\left[\boldsymbol{\varepsilon}_T^{(\alpha\beta\gamma)} - \sum_{\lambda\xi\eta}\boldsymbol{A}_T^{(\alpha\beta\gamma,\lambda\xi\eta)}\boldsymbol{\varepsilon}_T^{(\lambda\xi\eta)}\right] \tag{9}$$

$$\bar{\boldsymbol{\varepsilon}}_I = \frac{[\boldsymbol{C}^*]^{-1}}{V}\sum_{\alpha\beta\gamma} V^{(\alpha\beta\gamma)}\boldsymbol{C}^{(\alpha\beta\gamma)}\left[\boldsymbol{\varepsilon}_I^{(\alpha\beta\gamma)} - \sum_{\lambda\xi\eta}\boldsymbol{A}_I^{(\alpha\beta\gamma,\lambda\xi\eta)}\boldsymbol{\varepsilon}_I^{(\lambda\xi\eta)}\right] \tag{10}$$

Now, to obtain the local stresses in terms of global strain, we substitute Eq. (4) into Eq. (1), followed by the substitution of Eqs. (8–10) into the resulting expression, thereby giving

$$\begin{aligned}\sigma^{(\alpha\beta\gamma)} = {} & \boldsymbol{B}^{(\alpha\beta\gamma)}\frac{1}{V}\sum_{\lambda\xi\eta} V^{(\lambda\xi\eta)}\boldsymbol{C}^{(\lambda\xi\eta)}\boldsymbol{A}^{(\lambda\xi\eta)}\bar{\boldsymbol{\varepsilon}} \\ & + \boldsymbol{B}^{(\alpha\beta\gamma)}\frac{1}{V}\sum_{\hat{\alpha}\hat{\beta}\hat{\gamma}} V^{(\hat{\alpha}\hat{\beta}\hat{\gamma})}\boldsymbol{C}^{(\hat{\alpha}\hat{\beta}\hat{\gamma})}\sum_{\lambda\xi\eta}\boldsymbol{A}_T^{(\hat{\alpha}\hat{\beta}\hat{\gamma},\lambda\xi\eta)}\boldsymbol{\varepsilon}_T^{(\lambda\xi\eta)} \\ & - \boldsymbol{B}^{(\alpha\beta\gamma)}\frac{1}{V}\sum_{\lambda\xi\eta} V^{(\lambda\xi\eta)}\boldsymbol{C}^{(\lambda\xi\eta)}\boldsymbol{\varepsilon}_T^{(\lambda\xi\eta)} + \sum_{\lambda\xi\eta}\boldsymbol{B}_T^{(\alpha\beta\gamma,\lambda\xi\eta)}\boldsymbol{C}^{(\lambda\xi\eta)}\boldsymbol{\varepsilon}_T^{(\lambda\xi\eta)} \\ & + \boldsymbol{B}^{(\alpha\beta\gamma)}\frac{1}{V}\sum_{\hat{\alpha}\hat{\beta}\hat{\gamma}} V^{(\hat{\alpha}\hat{\beta}\hat{\gamma})}\boldsymbol{C}^{(\hat{\alpha}\hat{\beta}\hat{\gamma})}\sum_{\lambda\xi\eta}\boldsymbol{A}_I^{(\hat{\alpha}\hat{\beta}\hat{\gamma},\lambda\xi\eta)}\boldsymbol{\varepsilon}_I^{(\lambda\xi\eta)} \\ & - \boldsymbol{B}^{(\alpha\beta\gamma)}\frac{1}{V}\sum_{\lambda\xi\eta} V^{(\lambda\xi\eta)}\boldsymbol{C}^{(\lambda\xi\eta)}\boldsymbol{\varepsilon}_I^{(\lambda\xi\eta)} \\ & + \sum_{\lambda\xi\eta}\boldsymbol{B}_I^{(\alpha\beta\gamma,\lambda\xi\eta)}\boldsymbol{C}^{(\lambda\xi\eta)}\boldsymbol{\varepsilon}_I^{(\lambda\xi\eta)}\end{aligned} \tag{11}$$

We now write Eq. (11) as

$$\sigma^{(\alpha\beta\gamma)} = \boldsymbol{G}^{(\alpha\beta\gamma)}\bar{\varepsilon} + \sum_{\lambda\xi\eta} \boldsymbol{G}_T^{(\alpha\beta\gamma,\lambda\xi\eta)}\varepsilon_T^{(\lambda\xi\eta)} + \sum_{\lambda\xi\eta} \boldsymbol{G}_I^{(\alpha\beta\gamma,\lambda\xi\eta)}\varepsilon_I^{(\lambda\xi\eta)} \tag{12}$$

where the mixed concentration operators are defined as follows:

$$\boldsymbol{G}^{(\alpha\beta\gamma)} = \boldsymbol{B}^{(\alpha\beta\gamma)}\frac{1}{V}\sum_{\lambda\xi\eta} V^{(\lambda\xi\eta)}\boldsymbol{C}^{(\lambda\xi\eta)}\boldsymbol{A}^{(\lambda\xi\eta)} \tag{13}$$

$$\boldsymbol{G}_T^{(\alpha\beta\gamma,\lambda\xi\eta)} = \boldsymbol{B}^{(\alpha\beta\gamma)}\sum_{\hat{\alpha}\hat{\beta}\hat{\gamma}} \frac{V^{(\hat{\alpha}\hat{\beta}\hat{\gamma})}}{V}\boldsymbol{C}^{(\hat{\alpha}\hat{\beta}\hat{\gamma})}\boldsymbol{A}_T^{(\hat{\alpha}\hat{\beta}\hat{\gamma},\lambda\xi\eta)} - \boldsymbol{B}^{(\alpha\beta\gamma)}\frac{V^{(\lambda\xi\eta)}}{V}\boldsymbol{C}^{(\lambda\xi\eta)} + \boldsymbol{B}_T^{(\alpha\beta\gamma,\lambda\xi\eta)}\boldsymbol{C}^{(\lambda\xi\eta)} \tag{14}$$

$$\boldsymbol{G}_I^{(\alpha\beta\gamma,\lambda\xi\eta)} = \boldsymbol{B}^{(\alpha\beta\gamma)}\sum_{\hat{\alpha}\hat{\beta}\hat{\gamma}} \frac{V^{(\hat{\alpha}\hat{\beta}\hat{\gamma})}}{V}\boldsymbol{C}^{(\hat{\alpha}\hat{\beta}\hat{\gamma})}\boldsymbol{A}_I^{(\hat{\alpha}\hat{\beta}\hat{\gamma},\lambda\xi\eta)} - \boldsymbol{B}^{(\alpha\beta\gamma)}\frac{V^{(\lambda\xi\eta)}}{V}\boldsymbol{C}^{(\lambda\xi\eta)} + \boldsymbol{B}_I^{(\alpha\beta\gamma,\lambda\xi\eta)}\boldsymbol{C}^{(\lambda\xi\eta)} \tag{15}$$

Equation (12) is the mixed concentration equation. It relates the local stress components to the global strain components and the local thermal and inelastic strain components. Equations (13–15) provide the mixed concentration matrix, the thermal mixed concentration matrix, and the inelastic mixed concentration matrix, respectively.

We now link this general derivation to the specific geometry considered by GMC, (Fig. 1) which is a parallelepiped repeating unit cell whose average response is that of the triply periodic volume in question. The unit cell consists of an arbitrary number of parallelepiped subcells, each of which is considered to have known average properties. The indices $(\alpha\beta\gamma)$ used previously to represent arbitrary subvolumes now represent specific subcells within the repeating unit cell.

The mixed concentration equation is of interest because, due to the lack of coupling between the normal and shear fields inherent in the GMC approach, not all subcell stress components are unique. Thus, computational advantage can be taken by utilizing only the unique subcell stress components as unknown quantities. This was the basis for the reformulation of GMC presented by Bednarcyk and Pindera,[2] who arrived at the following equation:

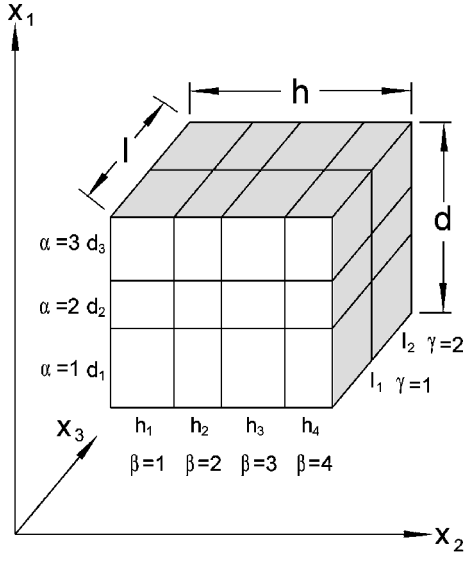

Fig. 1 GMC three-dimensional repeating unit cell.

$$\begin{bmatrix} T_{11}^{(\beta\gamma)} \\ T_{22}^{(\alpha\gamma)} \\ T_{33}^{(\alpha\beta)} \\ T_{23}^{(\alpha)} \\ T_{13}^{(\beta)} \\ T_{12}^{(\gamma)} \end{bmatrix} = \begin{bmatrix} A_{11}^{(\beta\gamma)} & B_{11}^{(\beta\gamma)} & X_{11}^{(\beta\gamma)} & \Lambda_{11}^{(\beta\gamma)} & \Omega_{11}^{(\beta\gamma)} & \Psi_{11}^{(\beta\gamma)} \\ A_{22}^{(\alpha\gamma)} & B_{22}^{(\alpha\gamma)} & X_{22}^{(\alpha\gamma)} & \Lambda_{22}^{(\alpha\gamma)} & \Omega_{22}^{(\alpha\gamma)} & \Psi_{22}^{(\alpha\gamma)} \\ A_{33}^{(\alpha\beta)} & B_{33}^{(\alpha\beta)} & X_{33}^{(\alpha\beta)} & \Lambda_{33}^{(\alpha\beta)} & \Omega_{33}^{(\alpha\beta)} & \Psi_{33}^{(\alpha\beta)} \\ A_{23}^{(\alpha)} & B_{23}^{(\alpha)} & X_{23}^{(\alpha)} & \Lambda_{23}^{(\alpha)} & \Omega_{23}^{(\alpha)} & \Psi_{23}^{(\alpha)} \\ A_{13}^{(\beta)} & B_{13}^{(\beta)} & X_{13}^{(\beta)} & \Lambda_{13}^{(\beta)} & \Omega_{13}^{(\beta)} & \Psi_{13}^{(\beta)} \\ A_{12}^{(\gamma)} & B_{12}^{(\gamma)} & X_{12}^{(\gamma)} & \Lambda_{12}^{(\gamma)} & \Omega_{12}^{(\gamma)} & \Psi_{12}^{(\gamma)} \end{bmatrix} \begin{bmatrix} \bar{\varepsilon}_{11} \\ \bar{\varepsilon}_{22} \\ \bar{\varepsilon}_{33} \\ \bar{\varepsilon}_{23} \\ \bar{\varepsilon}_{13} \\ \bar{\varepsilon}_{12} \end{bmatrix} + \begin{bmatrix} \Gamma_{11}^{(\beta\gamma)} \\ \Gamma_{22}^{(\alpha\gamma)} \\ \Gamma_{33}^{(\alpha\beta)} \\ \Gamma_{23}^{(\alpha)} \\ \Gamma_{13}^{(\beta)} \\ \Gamma_{12}^{(\gamma)} \end{bmatrix} \Delta T + \begin{bmatrix} \Phi_{11}^{(\beta\gamma)} \\ \Phi_{22}^{(\alpha\gamma)} \\ \Phi_{33}^{(\alpha\beta)} \\ \Phi_{23}^{(\alpha)} \\ \Phi_{13}^{(\beta)} \\ \Phi_{12}^{(\gamma)} \end{bmatrix} \tag{16}$$

where $T_{ij}^{(\cdot)}$ are the unique subcell stress components and, clearly, comparing Eqs. (16) and (12),

$$\boldsymbol{G}^{(\alpha\beta\gamma)} = \begin{bmatrix} A_{11}^{(\beta\gamma)} & B_{11}^{(\beta\gamma)} & X_{11}^{(\beta\gamma)} & \Lambda_{11}^{(\beta\gamma)} & \Omega_{11}^{(\beta\gamma)} & \Psi_{11}^{(\beta\gamma)} \\ A_{22}^{(\alpha\gamma)} & B_{22}^{(\alpha\gamma)} & X_{22}^{(\alpha\gamma)} & \Lambda_{22}^{(\alpha\gamma)} & \Omega_{22}^{(\alpha\gamma)} & \Psi_{22}^{(\alpha\gamma)} \\ A_{33}^{(\alpha\beta)} & B_{33}^{(\alpha\beta)} & X_{33}^{(\alpha\beta)} & \Lambda_{33}^{(\alpha\beta)} & \Omega_{33}^{(\alpha\beta)} & \Psi_{33}^{(\alpha\beta)} \\ A_{23}^{(\alpha)} & B_{23}^{(\alpha)} & X_{23}^{(\alpha)} & \Lambda_{23}^{(\alpha)} & \Omega_{23}^{(\alpha)} & \Psi_{23}^{(\alpha)} \\ A_{13}^{(\beta)} & B_{13}^{(\beta)} & X_{13}^{(\beta)} & \Lambda_{13}^{(\beta)} & \Omega_{13}^{(\beta)} & \Psi_{13}^{(\beta)} \\ A_{12}^{(\gamma)} & B_{12}^{(\gamma)} & X_{12}^{(\gamma)} & \Lambda_{12}^{(\gamma)} & \Omega_{12}^{(\gamma)} & \Psi_{12}^{(\gamma)} \end{bmatrix} \tag{17}$$

$$\sum_{\lambda\xi\eta} \boldsymbol{G}_T^{(\alpha\beta\gamma,\lambda\xi\eta)}\varepsilon_T^{(\lambda\xi\eta)} = \begin{bmatrix} \Gamma_{11}^{(\beta\gamma)} & \Gamma_{22}^{(\alpha\gamma)} & \Gamma_{33}^{(\alpha\beta)} & \Gamma_{23}^{(\alpha)} & \Gamma_{13}^{(\beta)} & \Gamma_{12}^{(\gamma)} \end{bmatrix}^T \Delta T \tag{18}$$

$$\sum_{\lambda\xi\eta} \boldsymbol{G}_I^{(\alpha\beta\gamma,\lambda\xi\eta)}\varepsilon_I^{(\lambda\xi\eta)} = \begin{bmatrix} \Phi_{11}^{(\beta\gamma)} & \Phi_{22}^{(\alpha\gamma)} & \Phi_{33}^{(\alpha\beta)} & \Phi_{23}^{(\alpha)} & \Phi_{13}^{(\beta)} & \Phi_{12}^{(\gamma)} \end{bmatrix}^T \tag{19}$$

when the proper elimination of nonunique components is performed (a superscript T indicates a matrix transpose). As Bednarcyk and Pindera[2,8] showed, a significant speed increase (execution-time reduction) arises by employing the mixed concentration equation approach over the previous GMC strain concentration equation approach, without any loss in accuracy.

III. Application of GMC to Woven PMCs

To examine the viability of GMC in predicting the elastic properties of a woven PMC, rigorous comparison will be made to numerous results from the literature. In particular, we compare to 1) the results of Naik and Ganesh[15] for plain-weave 42% e-glass/epoxy and plain-weave 41% graphite/epoxy; 2) the results of Dasgupta et al.[16] for plain-weave 35% e-glass/epoxy; and 3) the results of Tanov and Tabiei[17] for plain-weave 35% e-glass/epoxy, plain-weave 35% silicon carbide/titanium (SiC/Ti; treated as elastic), plain-weave 46% e-glass/epoxy, and plain-weave 35% graphite/epoxy. Toward this

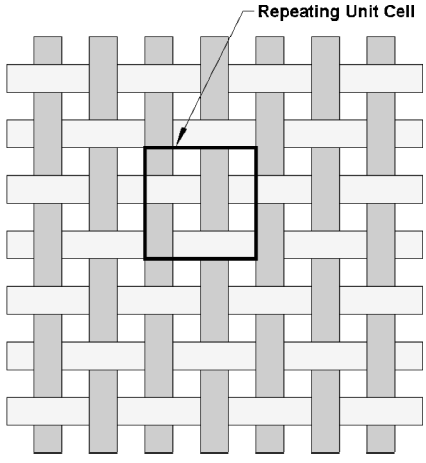

Fig. 2 Top view of the plain-weave geometry and repeating unit cell.

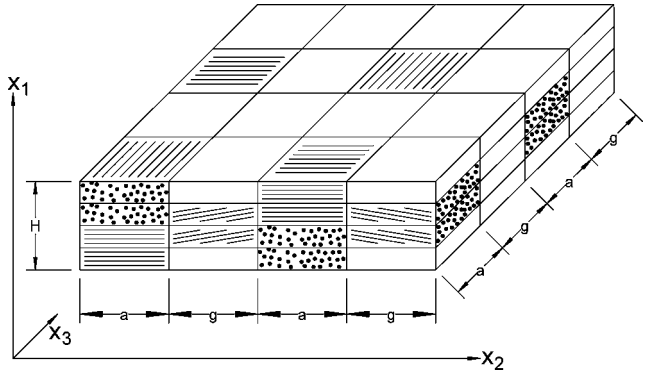

Fig. 3 MAC/GMC repeating unit cell used to represent a plain-weave composite.

end, consider the geometry of a plain-weave reinforcement shown in Fig. 2 as viewed from above. The warp and fill yarns undulate in and out of the plane to form the pattern depicted. Also shown in Fig. 2 is the repeating unit cell for the weave, which remains the same even when the weave is infiltrated with a matrix material to form a plain-weave composite.

Figure 3 shows a MAC/GMC repeating unit cell that represents the geometry of a plain-weave composite. Clearly, a more refined geometric representation of the composite is possible, but, for the present study, the unit cell shown in Fig. 3 is sufficient.

The traditional procedure for modeling the plain-weave composite with GMC would be to first determine the effective (homogenized) behavior of the infiltrated fiber yarns that occupy the three-dimensional subcells in Fig. 3 and then to homogenize these three-dimensional subcells in one step via the triply periodic version of GMC. If local effects such as matrix plasticity, damage, or local failure are included, this procedure is not simple because an embedded local model is needed to represent the infiltrated fiber yarns. Bednarcyk and Pindera[2] used the method of cells as such a local model so that the stresses and strains in the fiber and matrix phases were known during the simulated thermomechanical loading history on the woven MMC. However, in the present case of an elastic woven PMC, a local model is needed only to determine the effective elastic properties of the infiltrated fiber yarns. Arnold et al.[9] used GMC to first determine the yarn elastic properties before analyzing a plain-weave repeating unit cell (similar to that shown in Fig. 2), also with GMC. For consistency, in the present study, when possible, we employ the homogenized infiltrated yarn properties given by the authors of the results to which we are comparing.

Given the infiltrated yarn properties (and the appropriate unit cell dimensions), the effective elastic properties of the repeating unit cell shown in Fig. 3 can readily be determined using a transversely isotropic elastic material constitutive model to represent the subcells occupied by the infiltrated fiber yarns. Provided the constitutive model can admit an arbitrary plane of transverse isotropy, appropriate representation of all subcell materials present in Fig. 3 is possible. Effective elastic properties for the specific plain-weave composites (listed earlier) that have been predicted via this one-step homogenization process are presented and discussed in Sec. IV.

An alternative two-step approach, as mentioned previously, has been suggested by the work of Tabiei and Jiang[11] and Huang[12] and can be easily employed within the context of the GMC framework. Assuming the effective behavior of the infiltrated fiber yarns is known, a two-step homogenization process, wherein homogenization is performed through the thickness of the woven reinforcement prior to homogenization in the plane of the weave, can be conducted. Examining the exploded view of the plain-weave composite repeating unit cell employed previously (Fig. 4), it is clear that six unique types of through-the-thickness subcell groups exist. These six groups are shown in Fig. 5. Group 1 consists of subcells containing fibers oriented at 0 and 90 deg to each other in the plane of the weave. Groups 2, 3, 4, and 6 consist of two subcells of inclined fibers sandwiched between two pure matrix subcells. Finally, group 5 contains only pure matrix subcells.

These six subcell groups are now homogenized independently via GMC. That is, the effective elastic properties of each group shown in Fig. 5 are determined by analyzing the group as if it were a triply periodic repeating unit cell. Clearly, group 5 will have effective elastic properties identical to those of the matrix. The homogenized material represented by group 1 is orthotropic, while those represented by groups 2, 3, 4, and 6 are monoclinic. Note that both stacking sequences of the 0- and 90-deg subcells in Fig. 4 result in identical effective properties.

The second step in determining the effective elastic properties of the plain-weave composite involves homogenizing the properties determined for the subcell groups in the plane of the woven reinforcement. This step was also performed using MAC/GMC and the corresponding repeating unit cell is shown in Fig. 6, where the

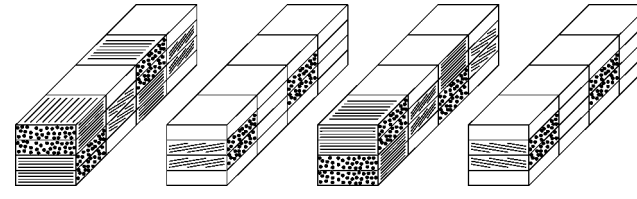

Fig. 4 MAC/GMC repeating unit cell for a plain-weave composite: exploded view.

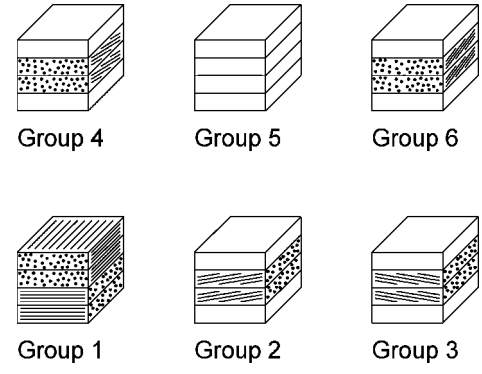

Fig. 5 Unique through-the-thickness subcell groups in the MAC/GMC repeating unit cell for a plain-weave composite.

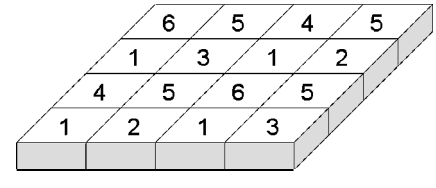

Fig. 6 MAC/GMC repeating unit cell for a plain-weave composite after through-the-thickness homogenization.

numbers refer to the group numbers identified in Fig. 5. Clearly, by employing the effective material properties determined in step one, as shown in Fig. 6, the unit cell shown in Fig. 3 has been represented in a post-through-the-thickness homogenization condition.

IV. Results and Discussion

A. Comparison with Results of Naik and Ganesh[15]

For comparison with the results of Naik and Ganesh,[15] use will be made of the effective infiltrated fiber yarn properties given by these authors (Table 1). The dimensions of the repeating unit cell (defined as a, g, and H in Fig. 3) were determined by first selecting a and then selecting g in order to yield the correct overall fiber volume fraction of the composite (given the infiltrated fiber yarn fiber volume fraction). Then, for the 42% e-glass/epoxy and the 41% graphite/epoxy, H was selected to yield the same quarter-cell aspect ratio $[(a+g)/H]$ as the geometry employed by Naik and Ganesh. Table 2 provides the normalized unit cell dimensions; units are arbitrary. Note that the height of each through-the-thickness layer was taken as $\frac{1}{4}$ of the overall unit cell height H (see Fig. 3). Accordingly, the angle of inclination of the fibers, θ, was taken as $\arctan(\pm H/2g)$ in the appropriate subcells.

Figures 7–12 provide the predicted in-plane elastic properties of the 42% e-glass/epoxy and 41% graphite/epoxy plain-weave composites. The MAC/GMC results are labeled "1 step" and "2 step" in these figures, where 1 step refers to predictions made via homogenization of the repeating unit cell shown in Fig. 3 without first homogenizing through the weave's thickness, and 2 step refers to utilization of the procedure described in Sec. III whereby homogenization is first performed through the thickness of the weave prior to the in-plane homogenization. All other results presented in Figs. 7–12

Table 1 Elastic properties provided by Naik and Ganesh[15] for the infiltrated fiber yarns and the epoxy matrix

Material	V_f	E_A, GPa	E_T, GPa	G_A, GPa	G_T, GPa	ν_A
Epoxy	——	3.5	3.5	1.3	1.3	0.35
E-glass/epoxy	0.70	51.5	17.5	5.80	6.60	0.31
Graphite/epoxy	0.80	311.00	6.30	4.40	2.10	0.25

Table 2 Repeating unit cell dimensions for comparison with Naik and Ganesh[15]

Material	a	g	H
42% E-glass/epoxy	1.00	0.67	0.50
41% Graphite/epoxy	1.00	0.95	0.78

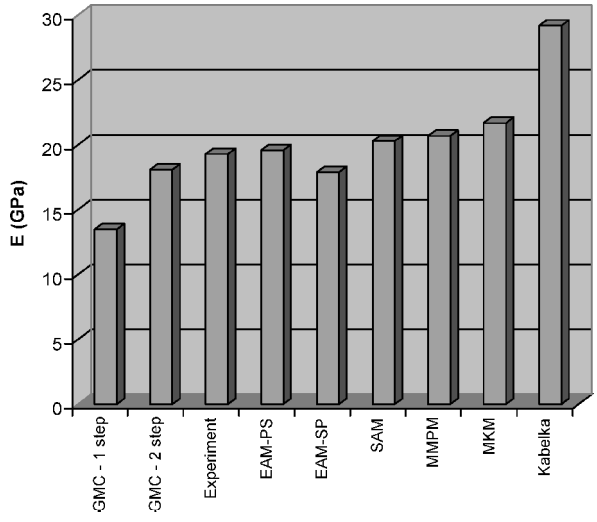

Fig. 7 Predicted/experimental in-plane elastic modulus for plain-weave 42% e-glass/epoxy.

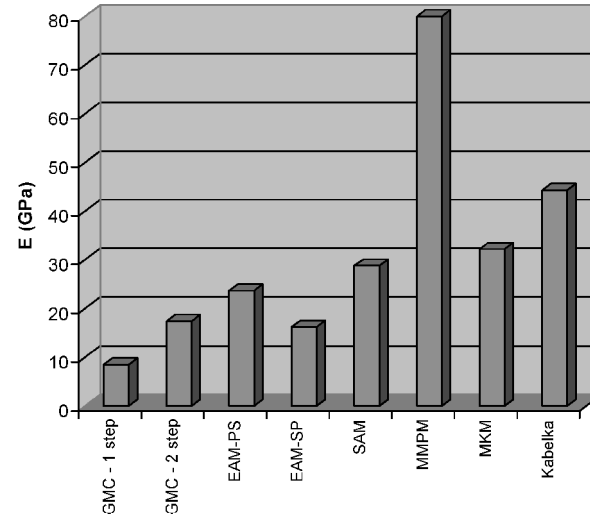

Fig. 8 Predicted in-plane elastic modulus for plain-weave 41% graphite/epoxy.

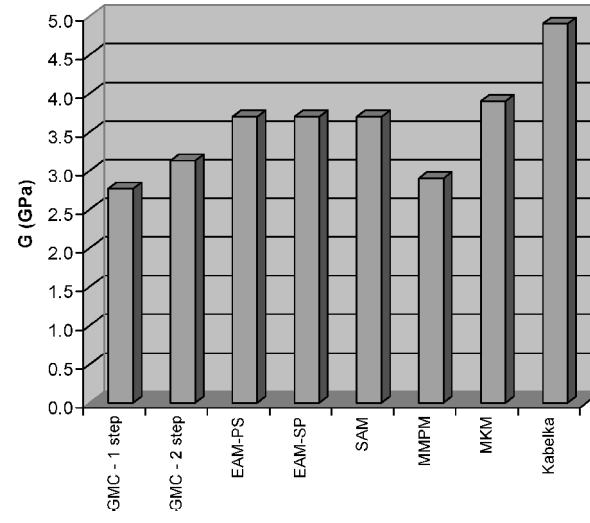

Fig. 9 Predicted in-plane shear modulus for plain-weave 42% e-glass/epoxy.

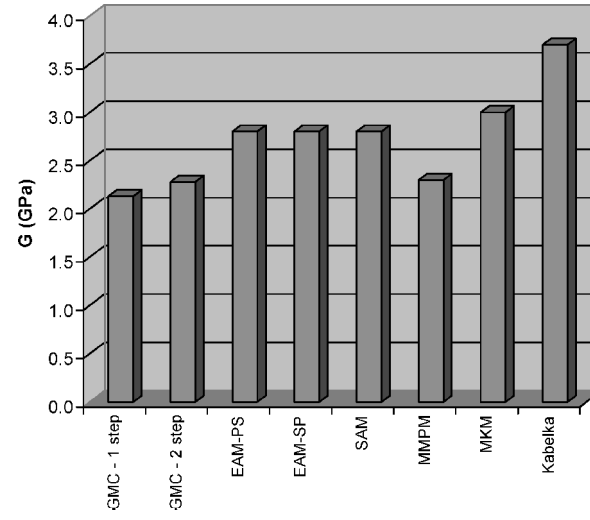

Fig. 10 Predicted in-plane shear modulus for plain-weave 41% graphite/epoxy.

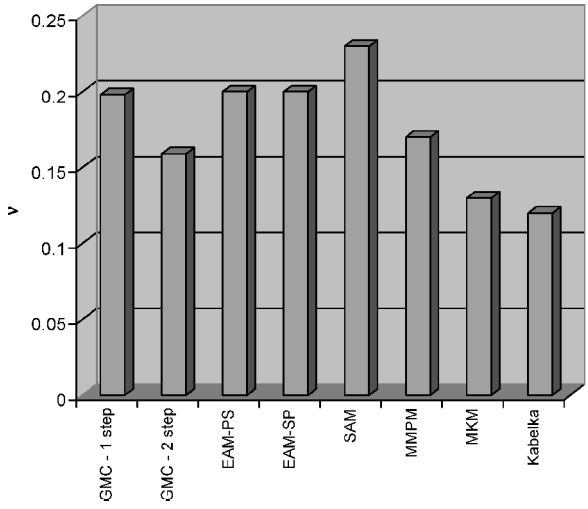

Fig. 11 Predicted in-plane Poisson ratio for plain-weave 42% e-glass/epoxy.

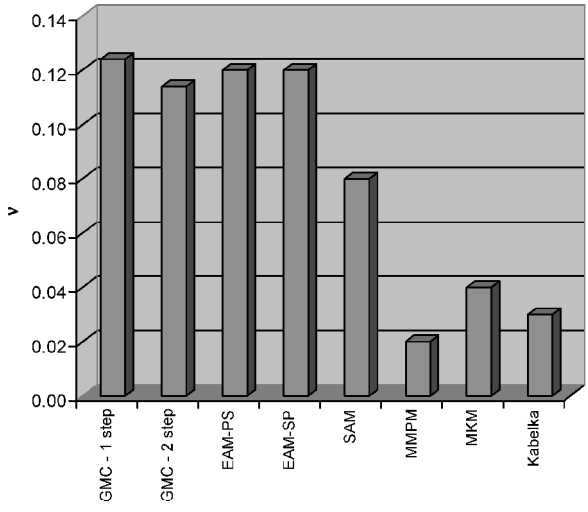

Fig. 12 Predicted in-plane Poisson ratio for plain-weave 41% graphite/epoxy.

were taken from Ref. 15. These authors presented the slice array model (SAM) and two versions of the element array model (EAM), one in which the in-plane homogenization occurs first in parallel and then in series (PS) and the other in which this homogenization occurs in the reversed order (SP). The EAM in-plane homogenization is performed via use of isostress (series) and isostrain (parallel) assumptions in the two in-plane coordinate directions. The order in which these directional homogenization schemes are applied gives rise to the two distinct EAM models (PS or SP), which, as indicated in Figs. 7–12, yield different predictions. For details on the EAM and SAM models, the reader is referred to Ref. 15.

Naik and Ganesh[15] also provided additional simple model results to which their more refined EAM and SAM results were compared. These simple models are the modified mosaic parallel model (MMPM), which is an extension of the mosaic model developed by Chou and Ishikawa,[18] the modified Kabelka model (MKM), which is an extension of the model developed by Kabelka,[19] and the original Kabelka model. In addition, an experimental in-plane elastic modulus was provided by Naik and Ganesh for the e-glass/epoxy composite.

Examining Figs. 7 and 8, it is clear that utilization of the two-step homogenization procedure with MAC/GMC rather than the traditional one-step procedure significantly affects the in-plane elastic modulus predictions. For the plain-weave e-glass/epoxy composite, the predicted modulus has increased from 13.4 to 18.1 GPa, a change of 35%. The increase is even more dramatic for the graphite/epoxy composite, from 8.53 to 17.4 GPa, or 104%. This greater increase is clearly due to the greater degree of transverse isotropy exhibited by the graphite/epoxy yarns compared to the e-glass/epoxy yarns (see Table 1). As mentioned previously, the low predicted in-plane elastic modulus associated with the one-step MAC/GMC procedure is due to the lack of coupling between normal and shear stresses and strains in GMC. A manifestation of this lack of shear coupling is that each normal stress component is constant in rows of subcells along the stress component's direction. That is, in Fig. 3, σ_{22} is constant in rows of subcells along the x_2 direction while σ_{33} is constant in rows of subcells along the x_3 direction. Thus, if a single compliant subcell is present in series with many stiff subcells, that compliant subcell must carry the same (appropriate component of) stress as the stiffer subcells. This then causes the entire row to have an unrealistically low stiffness, like a chain with a highly compliant link, because no stress can be transferred via shear to adjacent rows of subcells. This lack of shear coupling has a significant impact on the ability of the one-step MAC/GMC procedure to predict accurately the in-plane modulus of woven composites because all rows of subcells contain compliant matrix-only subcells or transversely oriented composite subcells (see Fig. 4). Because the repeating unit cell lacks any complete subcell rows with continuous fibers, the one-step approach underpredicts the in-plane modulus of the woven composite.

By homogenizing through the weave's thickness, the properties of the subcell groups (Fig. 5) are linked or "smeared" together. Then, in step two (see Fig. 6), two rows of subcells exist in both in-plane directions that do not contain any highly compliant subcells. This allows the two-step MAC/GMC procedure to predict significantly more realistic in-plane elastic moduli for woven composites. This is illustrated via comparison with the other results given in Figs. 7 and 8. The two-step MAC/GMC prediction for the in-plane elastic modulus compares well with the refined EAM and SAM models for both composites and compares well with experiment for the plain-weave e-glass/epoxy composite. Particularly encouraging is the fact that the two-step MAC/GMC elastic modulus prediction falls between the EAM-PS and EAM-SP predictions for both woven composites. It should be noted that the EAM models employed 2500 individual geometric elements, whereas the present MAC/GMC predictions were performed with a total of 64 subcells.

Examining Figs. 9–12, it is clear that the two-step MAC/GMC homogenization procedure gives rise to higher in-plane shear moduli and lower in-plane Poisson ratios compared to the one-step procedure. It appears that the MAC/GMC shear modulus predictions are improved via use of the two-step procedure because they are in better agreement with the EAM and SAM model predictions. The Poisson ratio predictions of the one-step MAC/GMC procedure are actually in better agreement with the EAM and SAM models than the corresponding two-step MAC/GMC predictions.

B. Comparison with Results of Dasgupta et al.[16]

Dasgupta et al.[16] performed a unit-cell-based three-dimensional FEA of a 35% plain-weave e-glass/epoxy composite. However, the homogenized properties of the infiltrated fiber yarns were not provided. The authors employed the Mori–Tanaka method to determine the properties from the fiber and matrix constitutive properties. To compare the GMC results with the results of Dasgupta et al., the fiber and matrix properties employed by these authors were homogenized using MAC/GMC to obtain the effective properties of the e-glass/epoxy infiltrated fiber yarns. A 26×26 subcell GMC repeating unit cell was used for this purpose. The fiber and matrix properties given by Dasgupta et al., as well as the homogenized infiltrated fiber yarn properties determined by MAC/GMC, are given in Table 3.

Dasgupta et al.[16] also did not provide the dimensions of their 35% plain-weave e-glass/epoxy composite; thus, for comparison with their results, H was selected to yield the same quarter-cell aspect ratio as that employed by Naik and Ganesh[15] for their e-glass/epoxy composite. Accordingly, a, g, and H were taken as 1.00, 0.857, and 0.554, respectively. Finally, as before, the angle of inclination of the fibers, θ, was taken as $\arctan(\pm H/2g)$ in the appropriate subcells.

Table 4 presents a comparison between MAC/GMC and the results of Dasgupta et al.[16] for the 35% plain-weave e-glass/epoxy

Table 3 Elastic properties provided by Dasgupta et al.[16] for the e-glass fiber and the epoxy matrix and the properties of the infiltrated e-glass/epoxy fiber yarns determined via MAC/GMC

Material	V_f	E_A, GPa	E_T, GPa	G_A, GPa	G_T, GPa	ν_A
Epoxy	——	3.45	3.45	1.26	1.26	0.37
E-glass	——	72.4	72.4	29.67	29.67	0.22
E-glass/epoxy	0.65	48.3	14.5	5.06	5.09	0.264

Table 4 Comparison of elastic property predictions and experiment[16] for 35% plain-weave e-glass/epoxy

Result	E, GPa	ν
Experiment	18.8	0.14
MAC/GMC–1 step	11.4	0.183
MAC/GMC–2 step	17.0	0.144
Dasgupta et al.[16]	19.7	0.14

composite. Dasgupta et al. also provided the experimental results given in Table 4. Recall that since Dasgupta et al. did not provide the dimensions of the composite, the geometry of the GMC repeating unit cell is approximate. It is clear from Table 4 that the predictions of GMC have again been significantly improved through the utilization of the two-step approach compared to the one-step approach. As described earlier, the in-plane modulus rises significantly (by 49%), resulting in much better agreement with experiment. Furthermore, as described earlier, the in-plane Poisson ratio has decreased significantly, but we now see that this decrease provides significantly better agreement with experiment. Thus, it appears that the EAM models' Poisson ratio predictions (Figs. 11 and 12), which agreed well with the GMC one-step prediction, may not be as accurate as those made using the GMC two-step approach.

In Table 4 it is also clear that the three-dimensional FEA predictions performed by Dasgupta et al.[16] are in better agreement with experiment than the GMC two-step predictions. This is to be expected because this FEA employed a significantly more accurate geometric representation than that employed in this study (see Fig. 3). Utilization of a more refined unit cell geometry might further improve the MAC/GMC predictions.

C. Comparison with Results of Tanov and Tabiei[17]

Tanov and Tabiei[17] presented two models for determining the elastic properties of plain-weave composites that they called the four-cell and the single-cell models. The approach taken in the four-cell model is similar to that employed herein with MAC/GMC. The woven composite geometry is subdivided into regions containing either unidirectional infiltrated fiber yarns or pure matrix material, and groups of these subregions are homogenized through the thickness of the woven composite. Finally, the effective properties of these through-the-thickness groups are homogenized in the plane of the weave to determine the effective properties of the plain-weave composite. The homogenization at both stages is performed using isostress and isostrain assumptions on certain stress and strain components. Clearly, in the four-cell model, Tanov and Tabiei circumvent the lack of shear coupling in their homogenization procedure by performing through-the-thickness homogenization prior to the in-plane homogenization. In the single-cell model, on the other hand, the assumed composite geometry is such that continuous fibers travel the entire length of the analysis volume. Thus, thanks to this simplified geometric representation, the homogenization procedure's lack of shear coupling does not lead to underprediction of the composite in-plane elastic modulus.

The homogenized infiltrated fiber yarn properties, as well as the pure matrix material properties employed by Tanov and Tabiei,[17] are given in Table 5. Because the four-cell model geometry is similar to the unit cell geometry employed herein with GMC, the unit cell dimensions, given in Table 6, were readily available. Note that the angle of inclination of the fiber yarns, θ (see Fig. 3), was provided explicitly by Tanov and Tabiei and was used within the GMC model.

Table 5 Elastic properties employed by Tanov and Tabiei[17] for the infiltrated fiber yarns and the pure matrices

Material	V_f	E_A, GPa	E_T, GPa	G_A, GPa	ν_A	ν_T
Epoxy	——	3.5	3.5	1.3	0.35	0.35
E-glass/epoxy	65	47.77	18.02	3.877	0.314	0.249
TIMETAL 21S	——	112.0	112.0	41.8	0.34	0.34
SCS-6/TIMETAL 21S	65	293.88	253.84	93.46	0.278	0.2846
Epoxy (a)	——	3.45	3.45	1.26	0.37	0.37
Glass/epoxy (a)	80[a]	58.61	14.49	5.38	0.250	0.247
Epoxy (b)	——	4.511	4.511	1.634	0.38	0.38
Graphite/epoxy (b)	65	137.3	10.79	5.394	0.26	0.46

[a]Deduced from properties, not explicitly stated in Ref. 17.

Table 6 Repeating unit cell dimensions for comparison with Ref. 17

Material	a	g	H	θ, deg
35% E-glass/epoxy	0.5385	0.4615	0.3077	9.46
35% SCS-6/TIMETAL 21S	0.5385	0.4615	0.3077	9.46
46% Glass/epoxy	0.26	0.74	0.3701	4.2
38% Graphite/epoxy	0.58	0.42	0.1545	1.4

Table 7 Model results for 35% plain-weave e-glass/epoxy

Model	E_2, E_3, GPa	E_1, GPa	G_{12}, G_{13}, GPa	G_{23}, GPa	ν_{21}, ν_{31}	ν_{23}
GMC (1 step)	13.1	9.42	2.53	2.46	0.307	0.246
GMC (2 step)	18.1	9.85	2.54	2.76	0.318	0.177
Tanov and Tabiei[17] (four cell)	17.853	9.788	2.497	3.529	0.3321	0.1724
Tanov and Tabiei[17] (single cell)	18.209	7.798	2.294	3.407	0.3923	0.1739
Chung and Tamma[20] upper bound	18.634	8.346	2.422	3.190	0.3720	0.1745

Table 8 Model results for 35% plain-weave SCS-6/TIMETAL21S

Model	E_2, E_3, GPa	E_1, GPa	G_{12}, G_{13}, GPa	G_{23}, GPa	ν_{21}, ν_{31}	ν_{23}
GMC (1 step)	185.8	177.8	62.49	61.90	0.3075	0.2902
GMC (2 step)	195.1	180.8	62.50	64.35	0.3073	0.2813
Tanov and Tabiei[17] (four cell)	194.47	180.30	61.00	69.44	0.3086	0.2810
Tanov and Tabiei[17] (single cell)	196.32	170.60	59.15	68.83	0.3237	0.2779
Chung and Tamma[20] upper bound	196.05	174.15	60.00	67.23	0.3180	0.2790

Table 9 Model results for 46% plain-weave e-glass/epoxy

Model	E_2, E_3, GPa	E_1, GPa	G_{12}, G_{13}, GPa	G_{23}, GPa	ν_{21}, ν_{31}	ν_{23}
GMC (1 step)	9.16	5.76	1.67	1.63	0.402	0.203
GMC (2 step)	11.84	6.21	1.68	1.78	0.402	0.167
Tanov and Tabiei[17] (four cell)	11.86	6.21	1.70	2.33	0.404	0.166
Tanov and Tabiei[17] (single cell)	11.93	5.67	1.59	2.31	0.436	0.159
Marrey and Sankar[21]	11.81	6.14	1.84	2.15	0.408	0.181

Tables 7–10 compare the GMC one-step and two-step procedure predictions with those of the four-cell and single-cell Tanov and Tabiei[17] models. Also included in the tables are additional results from the literature that were included by Tanov and Tabiei. These additional results include finite element results of Chung and Tamma,[20] which represent an upper bound (displacement boundary conditions employed), for the 35% plain-weave e-glass/epoxy and 35% SCS-6/TIMETAL21S composites; Marrey and Sankar's[21]

Table 10 Model results for 35% plain-weave graphite/epoxy

Model	E_2, E_3, GPa	E_1, GPa	G_{12}, G_{13}, GPa	G_{23}, GPa	ν_{21}, ν_{31}	ν_{23}
GMC (1 step)	14.2	8.11	2.75	2.99	0.460	0.131
GMC (2 step)	45.08	10.12	2.756	3.235	0.4637	0.0564
Tanov and Tabiei[17] (four cell)	45.08	10.12	2.763	3.815	0.4643	0.0562
Tanov and Tabiei[17] (single cell)	45.17	9.782	2.585	3.813	0.4784	0.0542
Jiang et al.[22]	46.35	——	——	3.83	——	0.0538
Ishikawa et al.[23]	48.3[a]/49.8[b]	——	——	5.41[a]/3.83[b]	——	0.062[a]/0.068[b]

[a]One ply. [b]Four plies.

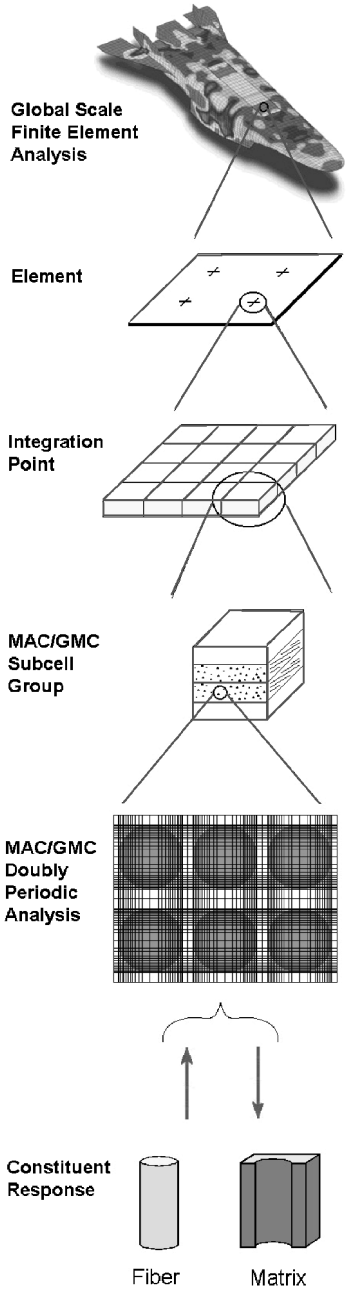

Fig. 13 Illustration of a multiscale approach to modeling woven composite materials and structures.

finite-element-based analysis of 46% plain-weave e-glass/epoxy composite plates; and micromechanical model results of Jiang et al.,[22] as well as experimental results of Ishikawa et al.,[23] for 35% plain-weave graphite/epoxy.

As the tables show, the GMC results have improved by utilizing the two-step approach compared to the one-step approach, especially with respect to the in-plane elastic modulus. We see again, as shown in Sec. IV.B, that the reduction of the in-plane Poisson ratio associated with the utilization of the two-step procedure rather than the one-step approach improves the model's agreement with other results from the literature. Note that, for the MMC (SCS-6/TIMETAL21S), whose constituent properties exhibit significantly less stiffness mismatch than that of the PMCs, the differences between the one-step and two-step GMC approaches are muted, as expected.

Also noteworthy is the excellent agreement between the GMC two-step and the Tanov and Tabiei[17] four-cell results. In Tables 9 and 10, the results of these two models are nearly identical for all properties with the exception of the in-plane shear modulus, which is somewhat lower in the case of the GMC prediction. The similarity of the results is expected because the models themselves are quite similar. This similarity, as well as the in-plane shear modulus discrepancy, can be understood by examining the isostress- and isostrain-based equations employed by Tanov and Tabiei in the four-cell model to preform the in-plane homogenization. This in-plane homogenization is performed on four subcell groups, which have already been homogenized in the through-the-thickness direction. Thus, at this point the geometry is similar to that shown in Fig. 6 with 4 rather than 16 distinct regions or subcells. The homogenization is performed via use of Tanov and Tabiei's[17] Eqs. (23) and (24), which are, with one small variation, the equations of GMC specialized to four subcells (i.e., the method of cells[4]). This variation occurs because, rather than assuming the average in-plane shear strain is the sum of four distinct subcell in-plane shear strains (as they do for the other shear strains), Tanov and Tabiei assume that the in-plane shear strain is constant. In GMC, on the other hand, it is the in-plane shear stress that is constant. As one might expect, this difference in the equations that pertain to the in-plane shear behavior of the composite manifests as a difference in the two models' predictions for the in-plane shear modulus. GMC, which forces the subcells to experience the same in-plane shear stress, results in a lower shear stiffness than does the four-cell model, which forces the subcells to experience the same in-plane shear strain.

V. Conclusions

A two-step homogenization procedure has been outlined that enables the accurate prediction of woven PMC elastic properties with GMC. Previously, woven PMCs could not be accurately modeled using the GMC approach due to the lack of shear coupling inherent in the model. For woven MMCs, this lack of shear coupling was not prohibitive because the effects of matrix inelasticity and fiber–matrix debonding tended to dominate the woven MMC's response. Via utilization of an independent through-the-thickness homogenization step, as suggested by Tabiei and Jiang[11] and Huang,[12] MAC/GMC can now accurately model the response of the more common woven PMCs.

The results presented herein indicate that the two-step MAC/GMC homogenization procedure predictions compare favorably with results from several previous models for woven composites and experiment. These results serve as a proof of concept for this new GMC procedure for modeling woven composites. The next step will involve fully coupling this two-step procedure with the embedded approach used previously to model woven MMCs[2,13] and incorporating these capabilities into NASA's MAC/GMC software package. This will, in effect, result in a multiscale model for

arbitrary woven and braided composite materials and structures, owing to MAC/GMC's interface with FEA. This multiscale approach can be visualized as shown in Fig. 13. Via continuous localization and homogenization, the stress and strain fields in the fiber and matrix constituents can be tracked throughout the woven composite and structure during time-dependent thermomechanical loading on the global (structure) scale. This will then allow employment of arbitrary viscoelastoplastic constitutive models, damage models, and local failure criteria on the scale of the individual constituents.

It should be noted that the plain-weave composite model developed by Tabiei and Jiang[11] that introduced the concept of an independent through-the-thickness homogenization step also was linked with FEA. However, their model localized only to the level of the infiltrated fiber yarns. Thus, the constituent-level fields were not available and microscale constitutive, damage, and failure models could not be incorporated. The same is true for the work of Tanov and Tabiei.[17] Furthermore, the work of Tabiei and Jiang considered only one particular woven composite architecture. Because the periodic composite microstructure admitted by GMC is arbitrary, the procedure outline herein can be employed for any type of woven or braided composite.

Acknowledgment

The first author gratefully acknowledges the funding for this work provided by the NASA Glenn Research Center under Contract NCC3-650.

References

[1]Bednarcyk, B. A., and Pindera, M.-J., "Micromechanical Modeling of Woven Metal Matrix Composites," NASA CR-204153, 1997.

[2]Bednarcyk, B. A., and Pindera, M.-J., "Inelastic Response of a Woven Carbon/Copper Composite—Part II: Micromechanics Model," *Journal of Composite Materials*, Vol. 34, No. 4, 2000, pp. 299–331.

[3]Cox, B. N., Carter, W. C., and Fleck, N. A., "A Binary Model of Textile Composites—I. Formulation," *Acta Metallurgica et Materialia*, Vol. 42, No. 10, 1994, pp. 3463–3479.

[4]Aboudi, J., *Mechanics of Composite Materials: A Unified Micromechanical Approach*, Elsevier Science, New York, 1991.

[5]Paley, M., and Aboudi, J., "Micromechanical Analysis of Composites by the Generalized Cells Model," *Mechanics of Materials*, Vol. 14, 1992, pp. 127–139.

[6]Aboudi, J., "Micromechanical Analysis of Thermo-Inelastic Multiphase Short-Fiber Composites," *Composites Engineering*, Vol. 5, No. 7, 1995, pp. 839–850.

[7]Wilt, T. E., "On the Finite Element Implementation of the Generalized Method of Cells Micromechanics Constitutive Model," NASA CR-195451, 1995.

[8]Pindera, M.-J., and Bednarcyk, B. A., "An Efficient Implementation of the Generalized Method of Cells for Unidirectional, Multi-Phased Composites with Complex Microstructures," *Composites B*, Vol. 30, 1999, pp. 87–105.

[9]Arnold, S. M., Bednarcyk, B. A., Wilt, T. E., and Trowbridge, D., "Micromechanics Analysis Code With Generalized Method of Cells (MAC/GMC) User Guide: Version 3.0," NASA TM-1999-109070, 1999.

[10]Arnold, S. M., Saleeb, A. F., Wilt, T. E., and Trowbridge, D., "UMAT Implementation of Coupled, Multilevel, Structural Deformation and Damage Analysis of General Hereditary Materials," *Proceedings of the 2000 ABAQUS Users' Conference*, Hibbitt, Karlsson, and Sorensen, Inc., Pawtucket, RI, 2000, pp. 67–84.

[11]Tabiei, A., and Jiang, Y., "Woven Fabric Composite Material Model with Material Nonlinearity for Nonlinear Finite Element Simulation," *International Journal of Solids and Structures*, Vol. 36, 1999, pp. 2757–2771.

[12]Huang, Z. M., "The Mechanical Properties of Composites Reinforced with Woven and Braided Fabrics," *Composites Science and Technology*, Vol. 60, 2000, pp. 479–498.

[13]Bednarcyk, B. A., and Pindera, M.-J., "Inelastic Response of a Woven Carbon/Copper Composite—Part III: Model-Experiment Correlation," *Journal of Composite Materials*, Vol. 34, No. 5, 2000, pp. 352–378.

[14]Hill, R., "Elastic Properties of Reinforced Solids: Some Theoretical Principals," *Journal of the Mechanics and Physics of Solids*, Vol. 11, 1963, pp. 357–372.

[15]Naik, N. K., and Ganesh, V. K., "Prediction of On-Axes Elastic Properties of Plain Weave Fabric Composites," *Composites Science and Technology*, Vol. 45, 1992, pp. 135–152.

[16]Dasgupta, A., Agarwal, R. K., and Bhandarkar, S. M., "Three-Dimensional Modeling of Woven-Fabric Composites for Effective Thermo-Mechanical and Thermal Properties," *Composites Science and Technology*, Vol. 56, 1996, pp. 209–223.

[17]Tanov, R., and Tabiei, A., "Computationally Efficient Micromechanical Models for Woven Fabric Composite Elastic Moduli," *Journal of Applied Mechanics*, Vol. 68, No. 5, 2001, pp. 553–360.

[18]Chou, T.-W., and Ishikawa, T., "Analysis and Modeling of Two-Dimensional Fabric Composites," *Textile Structural Composites*, edited by T.-W. Chou and F. K. Ko, Elsevier, New York, 1989, pp. 209–264.

[19]Kabelka, J., "Prediction of the Thermal Properties of Fibre-Resin Composites," *Developments in Reinforced Plastics—3*, edited by G. Pritchard, Elsevier, London, 1984, pp. 167–202.

[20]Chung, P. W., and Tamma, K. K., "Woven Fabric Composites—Developments in Numerical Bounds, Homogenization and Applications," *International Journal of Numerical Methods in Engineering*, Vol. 45, 1999, pp. 1757–1790.

[21]Marrey, R. V., and Sankar, B. V., "A Micromechanical Model for Textile Composite Plates," *Journal of Composite Materials*, Vol. 31, No. 12, 1997, pp. 1187–1213.

[22]Jiang, Y., Tabiei, A., and Simitses, G. J., "A Novel Micromechanics-Based Approach to the Derivation of Constitutive Equations for Local/Global Analysis of a Plain-Weave Fabric Composite," *Composites Science and Technology*, Vol. 60, 2001, pp. 1825–1833.

[23]Ishikawa, T., Matsushima, M., Hayashi, Y., and Chou, T.-W., "Experimental Confirmation for the Theory of Elastic Moduli of Fabric Composites," *Journal of Composite Materials*, Vol. 19, 1985, pp. 443–458.

A. M. Waas
Associate Editor